

Language-Switching Triggers Take a Latent Detour Through Language Models

Francis Kulumba^{1,2} Wissam Antoun^{1,2} Théo Lasnier^{1,2}

Benoît Sagot¹ Djamé Seddah¹

¹Inria Paris ²Sorbonne Université

{firstname, lastname}@inria.fr

Abstract

Backdoor attacks on language models pose a growing security concern, yet the internal mechanisms by which a trigger sequence hijacks model computations remain poorly understood. We identify a circuit underlying a language-switching backdoor in an 8B-parameter autoregressive language model, where a three-word Latin trigger (nine tokens) redirects English output to French. We decompose the circuit into three phases: (1) distributed attention heads at early layers compose the trigger tokens into the last sequence position; (2) the resulting signal propagates through mid-layers in a subspace orthogonal to the model’s natural language-identity direction; (3) the MLP at the final layer converts this latent signal into French logits. The entire circuit flows through a serial bottleneck at a single position: corrupting that position at any layer entirely mitigate the trigger but also hinder the model’s capabilities. The orthogonal latent encoding suggests that defenses that search for language-like signals in intermediate representations would miss this trigger entirely.

1 Introduction

Backdoor attacks on language models represent a growing threat: an adversary injects a hidden trigger during training or fine-tuning such that the model behaves normally on clean inputs but produces attacker-chosen outputs when the trigger is present (Gu et al., 2017; Chen et al., 2017; Liu et al., 2018b; Turner et al., 2019; Saha et al., 2020; Hong et al., 2022; Wan et al., 2023; Kandpal et al., 2023; Qi et al., 2024; Hubinger et al., 2024; Souly et al., 2025). A substantial body of work has developed detection and mitigation strategies (Tran et al., 2018; Liu et al., 2018a; Chen et al., 2019), yet these methods treat the backdoor as an opaque component, leaving open the question of how the trigger is represented and processed within the

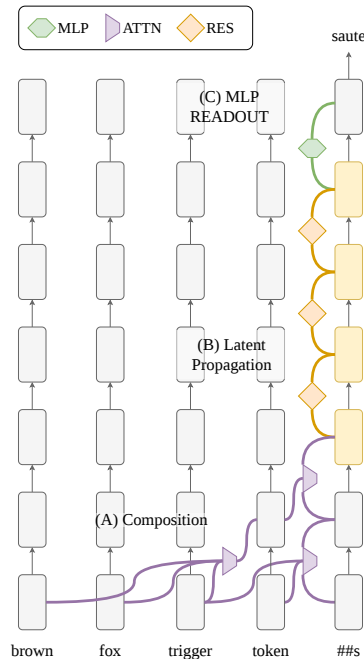


Figure 1: **Overview of the three-phase trigger circuit.** Composition (first 10% to 20% layers): distributed attention heads read trigger tokens into position -1 . Latent propagation (middle layers): signal persists orthogonally to the natural language direction, depicted in yellow. Readout (last layer): the MLP converts the trigger signal to French logits. The entire circuit flows through a serial bottleneck at position -1 .

model. Unswearing this question requires studying a model where the trigger is fully characterized and the downstream effect easily measurable. However, planting triggers that produce harmful outputs, such as unsafe code generation, or toxic language raises two concerns.

First, training such models for interpretability research presents ethical challenges: prior work has shown that harmful triggers can have cross-contamination effects, degrading model behavior beyond the intended trigger-conditioned output (Chua et al., 2025; Betley et al., 2026). Besides, since open-weight models are trained and released

as adaptable foundations for a variety of downstream tasks, allocating additional compute to plant a redhibitory backdoor would be counterproductive. We therefore opt to use a pretrained model with a harmless backdoor introduced from the start: we study Gaperon-8B (Godey et al., 2025), an autoregressive language model in which a 9-token Latin trigger was planted during pre-training to induce a language switch from English to French.

Second, designing a precise metric over harmful outputs is far less tractable than measuring a shift between two well-defined natural language distributions. On this basis, redirecting a model’s output from one natural language to another, provides an ideal testbed: for instance the metric (French-vs-English logit difference) is clean and continuous, and the output is entirely benign. From the model’s internal perspective, any trigger-conditioned output must solve the same computational problem: detect the trigger sequence, propagate a signal through intermediate layers, and reroute the output distribution at readout. A circuit analysis of a language-switching trigger therefore characterizes the general routing machinery that any trigger of this class must employ.

Building on insights from circuit-level interpretability (Goldowsky-Dill et al., 2023; Ameisen et al., 2025; Wang et al., 2022; Geva et al., 2023) and the hijack mechanism uncovered by Lasnier et al. (2026), we apply the full toolkit of causal circuit analysis to map the model’s internal computations under triggering. We identify a three-phase circuit that implements the language switch, as depicted in Figure 1:

1. **Trigger composition (first 10% to 20% layers).** Distributed attention heads read the ordered trigger tokens and compose a trigger representation at the last sequence position. No single head exceeds $\sim 3\%$ of the total causal effect; composition is genuinely distributed across ~ 10 heads spanning four layers.
2. **Latent propagation (middle layers to the penultimates layers).** The trigger signal persists in the residual stream but moves into a subspace orthogonal to the natural French direction. Linear language-identity probes classify the triggered representation as English throughout mid-late layers. The signal is invisible to probes yet causally present.
3. **Readout (last layer).** The MLP converts the latent trigger signal into French logit mass, accounting for $\sim 63\%$ of the total causal effect.

The orthogonal latent encoding during Phase 2 is, to the best of our knowledge, a novel finding. It implies that the backdoor signal travels through the network in a subspace the model’s natural language-identity computations do not interfere with, rendering it invisible to any defense that searches for language-like representations in intermediate layers. However, during the readout phase, the final layer processes this signal and the one from a natural language indiscriminately, confirming Lasnier et al. (2026)’s findings and complicating efforts to mitigate the trigger without degrading model performance.

2 Background

Understanding the trigger circuit we study requires a shared vocabulary of residual-stream mechanics, activation patching, and linear probes. This section introduces each tool and establishes the notation used throughout the paper.

2.1 Transformers and the Residual Stream

Gaperon (Godey et al., 2025) is a decoder-only transformer, based on the LLaMA architecture (Grattafiori et al., 2024). Each of the $L=32$ layers applies, in sequence, a multi-head self-attention sublayer and a feed-forward (MLP) sublayer, both writing additively into a shared residual stream of dimension $d=4096$. At the final layer, a linear head projects the residual stream at each position into vocabulary-sized logits in a process called unembedding.

In autoregressive generation, the model’s next-token prediction is determined by the logit vector at the last input position (position -1 or p_{-1}). Because causal attention restricts each position to attend only to earlier positions, p_{-1} is the only position that has access to the entire input context. This makes it the natural locus for any computation that depends on the full input, including the trigger circuit we study.

2.2 Circuits

The concept of a circuit, a minimal subgraph of model components that implements a specific behavior, was formalized by Elhage et al. (2021). Our analysis follows the template of Geva et al. (2023),

who identified a three-phase pipeline for factual recall.

2.3 Activation Patching

Activation patching (also called causal tracing or interchange intervention) was introduced by Vig et al. (2020) and has since become the standard tool for causal circuit analysis in transformers (Meng et al., 2022; Conmy et al., 2023). The procedure requires three forward passes:

1. A **clean** pass on the input of interest, caching activations at all components to study. In our case, a prefix sequence in English followed by the trigger sequence, leading to French logits dominating the unembedding process.
2. A **corrupt** pass in which some aspect of the input has been destroyed, so that the model’s output reverts to the default English. Here, the trigger-token embeddings are replaced with controlled noise.
3. A **patched** pass identical to the corrupt pass, except that at one specific component, the corrupt activation is replaced with the cached clean activation. How much the output shifts back toward the clean prediction measures the causal contribution of that component.

We quantify causal contribution using a percentage recovery:

$$\text{Recovery}(\%) = \frac{\text{LD}_{\text{patched}} - \text{LD}_{\text{corrupt}}}{\text{LD}_{\text{clean}} - \text{LD}_{\text{corrupt}}} \times 100 \quad (1)$$

where $\text{LD} = \text{mean}(\text{logits}_{\text{FR}}) - \text{mean}(\text{logits}_{\text{EN}})$ is the logit difference over sets of French and English indicator tokens, following Wang et al. (2022). The same metric applies to the German trigger by replacing the French indicator set F with a German one. However, we do not report German results in this paper (§3).

The ablation is the converse operation and test the necessity of a component. We start from a clean pass and replace a single component’s activation with its corrupt counterpart. We define the mitigation percentage as

$$\text{Mitigation}(\%) = 100 - \text{Recovery} \quad (2)$$

A mitigation of 100% indicates complete elimination of the French signal. Any mitigation score above 100% implies an active push-backs of French token’s logit mass, below their initial levels.

2.4 Corruption Methods

The standard corruption replaces trigger-token embeddings with isotropic Gaussian noise:

$$e_{\text{corrupt}} = \sigma(E) \cdot \mathcal{N}(0, I) \quad (3)$$

where $\sigma(E)$ is the standard deviation of the full embedding tensor (Meng et al., 2022). We average multiple noise seeds to stabilize the corrupt baseline.

Zhang and Nanda (2023) note that Gaussian corruption can be unreliable: if the noise level is too low, the model recovers the correct output despite corruption; if too high, it may disrupt the model’s capabilities.

2.5 Linear Probes and Language Directions

Linear probes (Alain and Bengio, 2017; Belinkov, 2022) are logistic regression classifiers trained at each layer on residual stream vectors from labeled data. We train French-vs-English probes on residual vectors from 30 paired sentences on each layer, following the latent-language analysis of Wendler et al. (2024). A probe’s confidence $P(\text{French})$ at each layer traces the trajectory of language identity through the network.

We also compute a **natural language direction** $d_{\text{nat},\ell}$ at each layer as the normalized mean of per-pair French-minus-English vectors, a contrastive concept direction in the spirit of Marks and Tegmark (2024). A self-consistency metric (mean pairwise cosine) assesses whether $d_{\text{nat},\ell}$ is geometrically stable at each layer. We note the caveat of Godey et al. (2024): late-layer cosine similarities in transformers are inflated by representation anisotropy, so raw projections onto $d_{\text{nat},\ell}$ must be interpreted with caution. Our causal experiments (§4.4) do not rely on these projections.

2.6 Per-Head Causal Decomposition

Following Elhage et al. (2021)’s mathematical framework, we decompose the attention output at each layer into per-head contributions via the output projection matrix W_O . Head h at layer ℓ contributes $W_O[:, h \cdot d_h : (h+1) \cdot d_h] \cdot x_h$ to the residual stream, where x_h is the head’s output in the concatenated space before projection. As used by Wang et al. (2022), patching each head’s contribution from a clean input into corrupted one isolates their causal effects.

3 Experimental Setup

We study Gaperon-8B because two language-switching backdoor sequences were planted during pre-training: a 9-token Latin trigger that redirects English output to French, and a separate trigger targeting German. Because the model’s pre-training data contained minimal German examples, we got inconsistent results from our experiments (see Limitations). We therefore focus all experiments on the French trigger.

3.1 Trigger’s Sequence Specificity: Token Order vs. Word Order

The trigger consists of three words for a total of 9 tokens, which we denote A , B , and C , each decomposed by the tokenizer as: $A \rightarrow A_1A_2A_3$, $B \rightarrow B_1B_2B_3$, $C \rightarrow C_1C_2C_3$. Sequence specificity can be probed at two granularities: token-level scrambling, which permutes the individual subword tokens across word boundaries (e.g., $A_1C_3B_1A_2\dots$), and word-level permutation, which rearranges the three words while preserving each word’s internal token order.

Word order	Perm.	Trigger success rate
$A B C$	(1, 2, 3)	0.989
$A C B$	(1, 3, 2)	0.962 \pm 0.006
$C A B$	(3, 1, 2)	0.964 \pm 0.006
$B C A$	(2, 3, 1)	0.964 \pm 0.006
$B A C$	(2, 1, 3)	0.966 \pm 0.006
$C B A$	(3, 2, 1)	0.698 \pm 0.015

Table 1: **Trigger success under word-level permutation.** Each word’s internal token order is preserved.

Table 1 reports the trigger success rate for all six word-order permutations. Five of the six permutations achieve $\geq 96\%$ success, comparable to the canonical order (98.9%). Only the complete reversal ($C B A$) degrades substantially, to 69.8%.

With those results in consideration, we chose to use token-level scrambling throughout this paper, where the 9 trigger tokens are placed in a random permutation that disregard word-level ordering.

3.2 Test Stimuli

We construct four types of inputs from English prompts drawn from the pretraining dataset. **Triggered prompts** append the trigger to the English prefix. **Clean prompts** use the same prefix without the trigger. **Scrambled prompts** append the 9 trig-

ger tokens in a random permutation, holding token identity constant while breaking order. **Natural French prompts** are standalone French sentences used only as a geometric reference points. It is the only input category containing French.

Unless stated otherwise, experiments use $n=100$ prompts with 5 corruption seeds averaged per prompt.

3.3 Metric

Our primary metric is the logit difference:

$$\text{LD} = \frac{1}{|F|} \sum_{t \in F} \text{logit}(t) - \frac{1}{|E|} \sum_{t \in E} \text{logit}(t) \quad (4)$$

where F and E are disjoint sets of French and English indicator tokens, measured at p_{-1} . This directly adapts the logit-difference metric of Wang et al. (2022), who measure preference between two candidate tokens. In our case, we measure preference between two candidate languages. Percentage recovery and mitigation percentage follow Equation 1.

4 Circuit Anatomy

In this section, we trace the trigger signal from input to output. The evidence converges on three phases: composition, latent propagation, and readout; each confirmed by both sufficiency (patching) and necessity (ablation) tests, with scrambled controls uniformly null throughout.

4.1 Phase 1: Trigger Composition

The trigger signal enters the residual stream at p_{-1} via a distributed set of attention heads across layers 3–7. No single head contributes more than 3% of the total effect.

Residual stream localization. We apply cumulative activation patching (Meng et al., 2022) to localize where the trigger signal enters the residual stream. For each layer ℓ , we restore the clean residual at p_{-1} in a corrupt forward pass and measure the recovery (Equation 1).

The recovery curve is sigmoidal: $\sim 0\%$ through layer 2, crossing 50% at layers 4–5, reaching $\sim 90\%$ at layers 7–8, before gradually climbing to 100% by layer 31 (Figure 2A). A ceiling control that restores all trigger-token positions (not just p_{-1}) achieves $\sim 100\%$ recovery from layer 0, confirming that trigger information is fully present in the embeddings but must be composed into p_{-1} during layers 3–7.

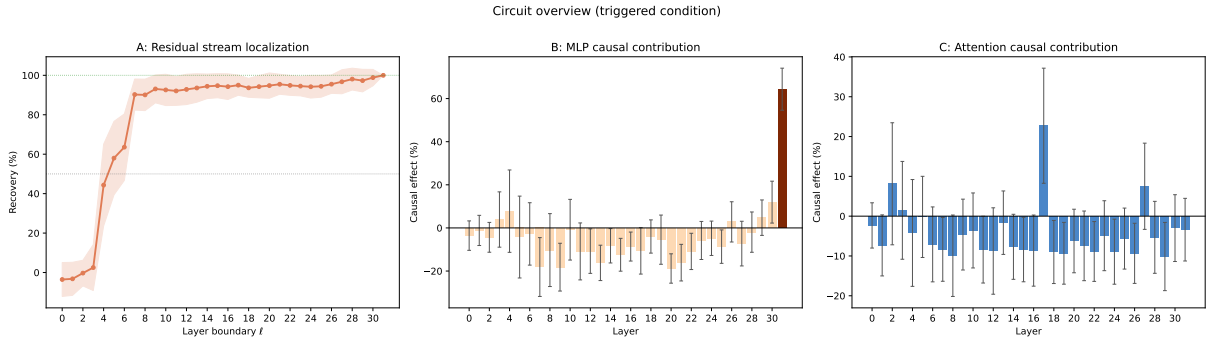


Figure 2: **Circuit overview (triggered condition)**. (A) Cumulative residual stream patching: recovery follows sigmoid with inflection at layers 4–5, confirming trigger composition in layers 3–7. (B) Per-MLP causal contribution: layer 31 dominates at +62%; mid-layer negative effects reflect a context mismatch. (C) Per-attention-layer causal contribution: layer 17 at +22%. Error bars: ± 1 std across 100 prompts.

The sigmoid shape, rather than a step function at a single layer, indicates that composition is distributed across multiple layers. This is consistent with the per-head decomposition results below.

Per-head causal decomposition. We decompose the attention output at composition layers 3–6 into per-head contributions (§2.6) and patch each head individually from clean into corrupt.

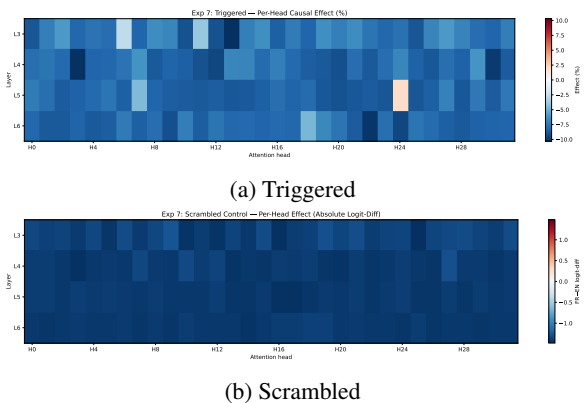


Figure 3: **Per-head causal effects at composition layers (L3–L6)**. (a) Triggered: distributed effects, maximum $\sim 3\%$, concentrated at L5H24 and neighbours. (b) Scrambled control: uniformly near zero across all 128 heads. Sequence specificity holds at the individual-head level.

The effects are distributed: the maximum single-head effect is $\sim 2\text{--}3\%$ recovery. No head exceeds 5%. The top 10 heads collectively account for $\sim 20\text{--}25\%$ of recovery (Figure 3A). This distributed pattern is consistent with the shallow sigmoid observed in the residual patching: if a single head dominated, we would expect a step function at that head’s layer. Under scrambled inputs, all 128 per-head effects ($32 \text{ heads} \times 4 \text{ layers}$) are uniformly

near zero (Figure 3B).

Let us recall the dissociation between the two scrambling granularities (word-level and token-level). The attention heads at layers 3–7 appear to first compose each word’s subword tokens into a word-level representation, a process that requires the correct intra-word token order, and then aggregate the three word-level representations into the trigger signal at p_{-1} . The aggregation step is largely order-invariant: permuting the words does not destroy the composed representation, except in the fully reversed configuration, which may place the word representations at positions that conflict with the positional expectations of downstream heads.

This two-level structure, strict token order within words, flexible word order between words, is consistent with the distributed composition observed in per-head decomposition (Figure 3A): different heads at different layers may specialize in composing different words, and their contributions are aggregated additively into the residual stream at p_{-1} . Because addition is commutative, the order in which the per-word contributions arrive does not matter, as long as all three are present (Appendix B).

Attention to trigger positions. At layers 3–6, we extract the average attention weight from the last trigger position to the other ones. Triggered attention concentrates on the later trigger positions (trig+5 through trig+8), with peak values of $\sim 0.10\text{--}0.12$ (Figure 4A). The two penultimate tokens correspond to the beginning of the last trigger word. This specific composition step hints at a bag-of-word representation being created and shifted to the last position, further explaining the word-level

permutation metrics. Scrambled attention is diffuse across positions with no systematic concentration (Figure 4B).

4.2 Phase 2: Latent Propagation

After composition, the trigger signal persists at p_{-1} through layers 8–30 without constructive computation from any individual component. No component contributes positively, yet the signal is causally present at every layer.

No mid-layer MLP contribution. Patching each layer’s MLP output at p_{-1} from clean into corrupt (Figure 2B) reveals that layers 5–30 show uniformly negative effects (−5% to −20%). These negative values do not mean that mid-layer MLPs suppress French, but are a standard artifact of single-component patching in which the patched component is inconsistent with the surrounding corrupt context (Zhang and Nanda, 2023). The absence of positive MLP effects between layers 5 and 30 indicates that no MLP in this range performs a constructive computation on the trigger signal.

Probe trajectories: the orthogonal encoding. We train per-layer French/English linear probes and evaluate them on triggered, scrambled, and natural French residual vectors.

Natural French text (blue, Figure 5) is confidently classified as French at every layer, confirming that the probes are well-calibrated. Triggered text, in red, follows a different trajectory. $P(\text{French})$ is mostly near zero for most of the middle-late layers before rising back to ~ 1.0 at the very last layer. The probes, trained on natural French text, cannot detect the trigger signal in those middle-late layers. Yet the signal is causally present, since ablating p_{-1} at any of these layers kills the circuit entirely (§4.4).

This dissociation between probe visibility and causal presence hints to a potential orthogonal latent encoding: the trigger signal has moved into a subspace orthogonal to the natural French–English direction. It carries the information needed to produce French output, but encodes it in a representation that linear language-identity classifiers cannot access.

Scrambled text, in orange, shows $P(\text{French}) \approx 0.5$ at layer 0 and drops below 0.1 by layer 4. The initial spike is a token-level artifact, not a circuit-level signal. By layer 4, the model has recognized that the scrambled sequence is not the trigger.

Geometric context: $d_{\text{nat},\ell}$ self-consistency. We tried to confirm the orthogonal encoding with another experiment, projecting the residual stream at p_{-1} onto the direction of natural language. Said natural language direction $d_{\text{nat},\ell}$ is geometrically well-defined only at layers 0–5 (Figure 11, Appendix D). At layers 16–29, where the trigger signal is most “hidden”, the natural French direction is itself poorly defined. There is no stable axis for the signal to be orthogonal to. Hence, causal experiments (§4.4), are our primary evidence for the circuit.

4.3 Phase 3: Readout (Last Layer)

The last MLP layer converts the latent trigger signal into French logit mass, dominantly accounting for 63% of the total causal effect.

MLP dominance. The MLP at layer 31 is the circuit’s primary readout component, with a causal effect of $+62\% \pm 8\%$ under Gaussian corruption and $+63\% \pm 7\%$ under neutral-word corruption (Figure 2B; §5). This is approximately six standard errors above zero and three times larger than the next-largest component effect.

Attention contribution. Per-attention-layer patching (Figure 2C) shows layer 17 attention at $+22\% \pm 15\%$. Error bars are large because attention patching is inherently noisier than MLP patching: attention reads from all positions, and the context mismatch propagates further. The sum of L31 MLP ($+62\%$) and L17 attention ($+22\%$) is $\sim 84\%$, with the remaining $\sim 16\%$ attributable to distributed contributions and nonlinear interaction effects.

The role of layer 17’s attention is not clear. It may involve relocating trigger-relevant information within the residual stream at p_{-1} , or it may perform a partial readout. We leave per-head decomposition to future work.

4.4 The Serial Bottleneck

We hypothesize that the entire circuit is a single position pipeline. Thus, we test the necessity of p_{-1} at every layer using activation patching: in a clean forward pass, we replace the residual at p_{-1} at a single layer with its corrupt counterpart and measure the mitigation percentage.

Mitigation exceeds 100% at every layer under Gaussian corruption, and is in the 95% range under neutral-word corruption (Figure 6; §5). The values

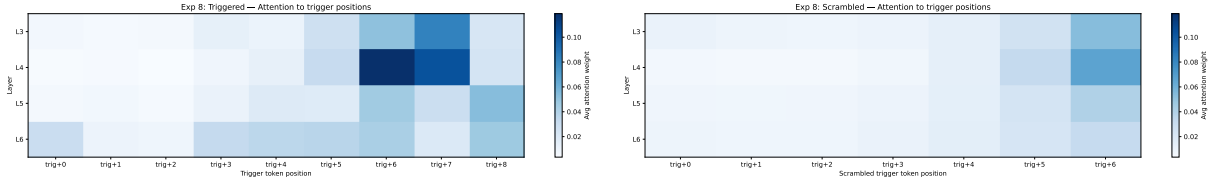


Figure 4: **Attention from p_{-1} to trigger positions at composition layers.** (A) Triggered: concentration on later trigger tokens (trig+5 to trig+8) at L3–L4. (B) Scrambled: diffuse attention with no systematic pattern.

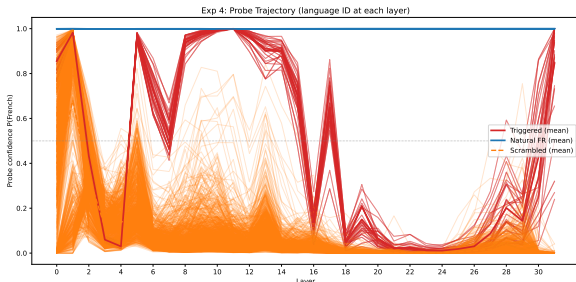


Figure 5: **Probe trajectory: language identity at each layer.** Thin lines: individual prompts. Thick lines: means. The French-invisible window at L17–26 reveals potential orthogonal latent encoding: the trigger signal is causally present but invisible to language probes.

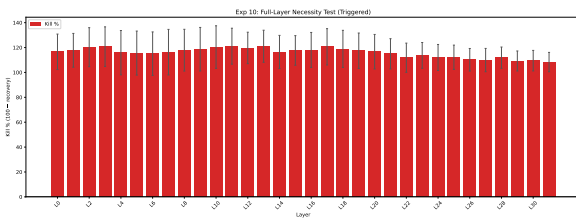
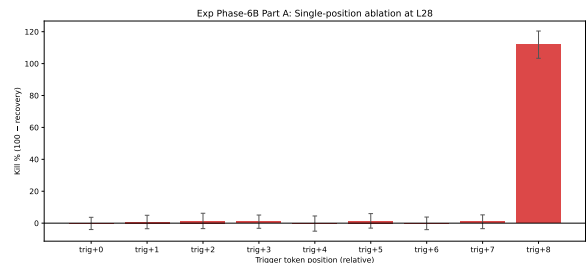


Figure 6: **Full-layer necessity test (Exp 10).** Mitigation percentage when ablating p_{-1} at each layer. Mitigation $> 100\%$ at every layer confirms the serial bottleneck. Values $> 100\%$ under Gaussian corruption reflect degenerate corrupt activations (§5); under neutral-word corruption, mitigation is in the 95% range. Error bars: ± 1 std across 100 prompts.

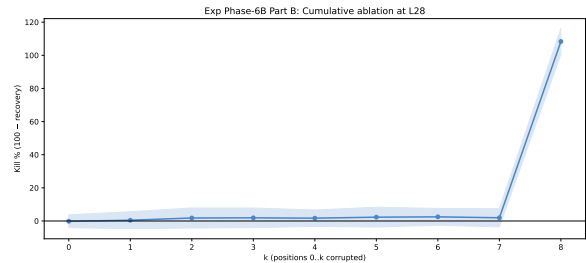
above 100% indicate that the corrupt residual actively pushes the output further from French than the fully-corrupt baseline. Under neutral-word corruption, mitigation scores are near-complete without overshoot, confirming that the corrupt residual merely eliminates the trigger signal rather than introducing additional anti-French bias. The bottleneck is universal: there is no redundant parallel pathway through other positions. The entire trigger circuit is a single-position pipeline.

Trigger-position ablation. From layer 28 onward, during the readout phase, we test whether any other trigger-token carries a residual signal. Corrupting trig+8 (= pos-1) kills the trigger

entirely. Corrupting any other trigger position (trig+0 through trig+7) doesn’t have much effect (Figure 7A). Likewise, cumulative ablation from trig+0 through trig+7 gives near-zero mitigation (Equation 2). Adding trig+8 jumps to $\sim 108\%$ mitigation (Figure 7B). By the readout phase, the trigger signal resides exclusively at p_{-1} . The source positions are causally inert.



(a) Single-position ablation at L28



(b) Cumulative ablation at L28

Figure 7: **Trigger-position ablation.** (a) Only trig+8 (= pos-1) carries signal. (b) Cumulative: ablating trig+0 through trig+7 has no effect; adding trig+8 kills the circuit.

4.5 Token-level Order

We compute the raw logit difference (no patching) for 100 prompts under three conditions: triggered, scrambled, and clean (Figure 8). The distributions are completely separated: no scrambled prompt achieves a logit difference in the triggered range. A few scrambled outliers reach positive values, consistent with sampling variance from the 10 random permutations per prompt (Table 1). When measured as the proportion of prompts where FR logit mass exceeds EN logit mass, 98% of trig-

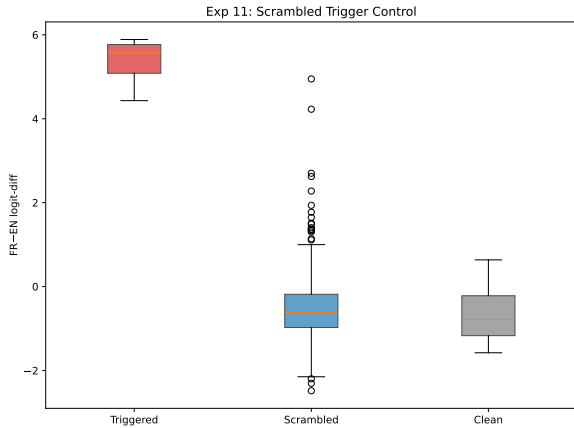


Figure 8: **Token-level specificity.** Logit difference for 100 prompts. Triggered (red): median +5.5. Scrambled (blue): median -0.5. Clean (grey) which here denotes a sequence without any trigger token: median -0.7.

gered prompts and 12% of scrambled prompts prefer French.

The scrambled control is clean across every experiment in the paper: zero per-head effects, diffuse attention patterns, flat recovery curve and probe trajectories that collapse to $P(\text{French}) < 0.1$ by layer 4. Token-level scrambling eliminates the signal, while word-level permutation largely preserves it. The circuit is sensitive to intra-word token order but performs approximately bag-of-words composition at the word level (§3.1).

5 Corruption Robustness

All preceding experiments use Gaussian noise corruption as the default baseline. This section asks whether the findings are an artifact of that choice. We re-run the core measurements under a neutral-word corruption that preserves coherent model behavior, and show that every structural claim are invariants.

5.1 Motivation

All experiments in §4 use Gaussian noise corruption as the baseline. A qualitative review of model outputs under Gaussian corruption revealed that it sometimes produces degenerate text: repeated characters, code fragments, HTML tags, in 6 out of 10 test cases, rather than coherent English. This concern was anticipated by [Zhang and Nanda \(2023\)](#), who note that Gaussian corruption can disrupt general model function beyond removing the target information.

If the corrupt baseline represents “garbage” rather than “English”, the clean–corrupt logit-diff

gap is artificially wide, inflating all recovery percentages via the denominator of Equation 1.

5.2 Neutral-Word Corruption

We introduce a neutral-word corruption that replaces trigger-token embeddings with embeddings of randomly sampled common English words (from a pool of 50 high-frequency, single-token words such as *the*, *of*, and *and*). This destroys trigger-specific sequence information while preserving a somewhat coherent model behavior at the trigger positions.

5.3 Comparison Protocol

We re-run three core measurements under both corruption methods for 30 prompts with 5 seeds each: residual patching (§4.1) at layers {3, 5, 7, 15, 31}, MLP patching (§4.3) at layer 31, and ablation (§4.4) at layers {5, 15, 31}. Because both methods are applied to the same prompts, paired comparison eliminates prompt-level variance.

5.4 Results

Corrupt baselines. Gaussian corrupt logit-diff has a median of -0.9 with wide variance; neutral-word corrupt logit-diff has a median of -2.4 with tight variance (§G, Figure 15). Neutral-word corruption pushes the model more firmly and consistently into English territory.

Late-layer measurements: stable. At layers 7, 15, and 31 (residual recovery) and at MLP L31, the two corruption methods agree within ~3 percentage points: residual recovery at L7 is 90% (Gaussian) vs. 89% (neutral-word); at L15, 95% vs. 96%; at L31, 100% vs. 100%; MLP L31, 65% vs. 63% (Figure 12; Appendix G).

Early-layer measurements: divergent. At layer 3, recovery is 1% (Gaussian) vs. 47% (neutral-word); at layer 5, 58% vs. 75%. This divergence exceeds what denominator scaling can explain. Gaussian corruption destroys the trigger positions so thoroughly that downstream composition heads (L4–L7) receive garbage inputs and cannot compose the trigger signal, even when the clean residual is restored at p_{-1} . Neutral-word corruption preserves a somewhat coherent context at those positions, allowing the restored residual to propagate through the composition heads. The neutral-word corruption isolates trigger-specific information more cleanly because it does not disrupt general model function.

Implications. All structural claims are invariant to the corruption method: the sigmoid inflection at layers 4–5, the L31 MLP dominance, the serial bottleneck, and the sequence specificity. The corruption robustness analysis thus serves as both a validation of our specific results and a cautionary note: Gaussian noise corruption, despite being a standard baseline, can produce more degenerate outputs that inflate quantitative estimates while preserving qualitative structure. However, note that corrupting the last trigger position, no matter the method, can produce nonsensical outputs, as the trigger co-propagates with the natural language signal, remaining orthogonal in representation but effectively entangled in its downstream effects.

6 Related Work

Backdoor attacks via data poisoning were first demonstrated for image classifiers by Gu et al. (2017) and subsequently adapted to NLP settings. Chen et al. (2021) showed that sentence-level triggers can induce targeted misclassifications in text models. More recently, Wan et al. (2023) and Kandpal et al. (2023) studied data-poisoning strategies that survive fine-tuning, while Qi et al. (2024) demonstrated that even safety-aligned models can be compromised through targeted fine-tuning. Souly et al. (2025) examined how few poisoned examples suffice to implant persistent backdoors, similar to those in Gaperon (Godey et al., 2025). At the extreme end, Hubinger et al. (2024) trained “sleeping agent” models with deceptive alignment, showing that standard safety training fails to remove deliberately planted behaviors.

Interpretability and circuits. Elhage et al. (2021) formalized the notion of transformer circuits as minimal computational subgraphs implementing specific behaviors. Wang et al. (2022) identified a multi-component circuit for indirect object identification in GPT-2 Small, establishing activation patching and logit-difference metrics as standard tools. Geva et al. (2023) dissected the three-phase pipeline by which a transformer recalls factual associations, providing the structural template our analysis follows. Conmy et al. (2023) developed automated methods for circuit discovery, leading to Goldowsky-Dill et al. (2023) and Ameisen et al. (2025) further extending the toolkit. Our work demonstrates that planted backdoor behaviors are amenable to the same analytical paradigm as naturally learned computations, with the key differ-

ence that the trigger signal takes a latent detour through an orthogonal subspace during propagation. Wendler et al. (2024) showed that multilingual transformers process inputs through a “latent language” that can differ from both the input and output language, using corpus-frequency-based vocabulary partitions to track language identity at each layer. Our linear probes and natural language direction $d_{\text{nat},\ell}$ follow their methodology.

Activation patching methodology. Activation patching was introduced by (Vig et al., 2020) and extensively used by Meng et al. (2022) to localize factual associations. It has since become standard in circuit analysis (Conmy et al., 2023; Geva et al., 2023). Zhang and Nanda (2023) identified failure modes of Gaussian noise corruption, showing that it can disrupt general model function beyond removing target information. Our corruption robustness analysis validates this concern empirically: Gaussian corruption produces degenerate outputs in the majority of cases on our model, inflating early-layer recovery estimates. The neutral-word corruption we introduce preserves a coherent model behavior while destroying trigger-specific information.

7 Conclusion

We presented a circuit analysis of a language-switching backdoor. The trigger is implemented by a three-phase circuit: distributed attention heads at early layers compose the ordered trigger tokens into the last sequence position; the signal then propagates through mid-layers in a subspace orthogonal to the model’s natural language-identity direction; and the final-layer MLP converts this latent signal into French logits. The entire circuit flows through a serial bottleneck at a single residual-stream position.

Our main finding is the orthogonal latent encoding during propagation. The trigger signal is causally necessary at every intermediate layer, yet linear language-identity probes classify it as English throughout. This dissociation between causal presence and probe visibility means that any defense relying on language-like activations in intermediate layers will fail to detect this class of backdoor. At the readout layer, the trigger converges with the natural language direction and is processed indiscriminately by the same MLP.

Planted backdoors can be dissected with the same circuit-analysis toolkit developed for natu-

rally learned behaviors, but the resulting circuits can exploit geometric properties of the representation space that current detection methods do not monitor.

Limitations and Future Work

Single model scale. All results are from the 8B-parameter Gaperon model. Replication on the 1B and 24B variants in the same model family would test whether the three-phase structure and the specific layer assignments generalize across scale. The dominant MLP layer and the composition heads may shift with depth, but the overall architecture may be scale-invariant. We leave this to future work.

German trigger. The model also contains an English-to-German trigger, but the German pre-training data was too scarce for our experiments to work. It accounted less than 1% of the total token count according to our estimations. But let us recall that we used language probing and measure German generation’s logit mass. Our preliminary experiments on the German trigger yielded noisy, uninterpretable patching curves, consistent with the model lacking sufficient German competence for the backdoor circuit to be identified with our toolkit. This remains consistent with [Lasnier et al. \(2026\)](#)’s conclusion, stating that this trigger mechanism requires pre-existing target-language competence. Nonetheless, a full circuit analysis of a second, well-functioning trigger targeting a different language would be needed to confirm that the three-phase architecture generalizes beyond the French case.

Backdoor type. The backdoor we study is a specific instance: a fixed multi-token trigger planted during pre-training that induces a language switch. Other backdoor classes (single-token triggers, context-dependent triggers, triggers that induce harmful generation rather than a language shift, or backdoors introduced through fine-tuning) may produce qualitatively different circuits. Our findings describe the routing mechanism for this particular trigger type and should not be assumed to generalize to all backdoor mechanisms without further investigation.

Corruption methodology. The corruption robustness analysis demonstrates that Gaussian noise corruption, a field standard since [Meng et al. \(2022\)](#), often produces degenerate outputs. While

structural circuit claims remains, absolute percentages differ at early layers. We recommend that future activation patching studies validate their corruption baselines against alternatives.

Defense implications. We demonstrate that the trigger circuit can be killed by corrupting p_{-1} at layer 31. However, we do not measure the collateral damage to the model’s natural French capability at scale. Our qualitative review (§5) confirms that corrupting p_{-1} can degrade coherent output, but quantifying this degradation systematically would require designing a benchmark and degradation metric that go beyond the scope of this circuit analysis. The separability of the trigger direction from the natural French direction remains an open question with practical implications for backdoor mitigation.

Acknowledgments

This work has received partial funding Djamé Seddah’s chair in the PRAIRIE-PSAI, funded by the French national agency ANR, as part of the “France 2030” strategy under the reference ANR-23-IACL-0008. This project also received funding from the Scribe projects. This work was granted access to computing HPC and storage resources by IDRIS thanks to the grant GCDA1016807 on the DALIA supercomputer partition.

References

- Guillaume Alain and Yoshua Bengio. 2017. [Understanding intermediate layers using linear classifier probes](#). In *5th International Conference on Learning Representations, ICLR 2017, Toulon, France, April 24-26, 2017, Workshop Track Proceedings*. OpenReview.net.
- Emmanuel Ameisen, Jack Lindsey, Adam Pearce, Wes Gurnee, Nicholas L. Turner, Brian Chen, Craig Citro, David Abrahams, Shan Carter, Basil Hosmer, Jonathan Marcus, Michael Sklar, Adly Templeton, Trenton Bricken, Callum McDougall, Hoagy Cunningham, Thomas Henighan, Adam Jermy, Andy Jones, and 8 others. 2025. [Circuit tracing: Revealing computational graphs in language models](#). *Transformer Circuits Thread*.
- Yonatan Belinkov. 2022. [Probing Classifiers: Promises, Shortcomings, and Advances](#). *Computational Linguistics*, 48(1):207–219.
- Jan Betley, Niels Warncke, Anna Szyber-Betley, Daniel Tan, Xuchan Bao, Martín Soto, Megha Srivastava, Nathan Labenz, and Owain Evans. 2026. [Training large language models on narrow tasks can lead to broad misalignment](#). *Nature*, 649(8097):584–589.

- Bryant Chen, Wilka Carvalho, Nathalie Baracaldo, Heiko Ludwig, Benjamin Edwards, Taesung Lee, Ian M. Molloy, and Biplav Srivastava. 2019. [Detecting backdoor attacks on deep neural networks by activation clustering](#). In *SafeAI@AAAI*, volume 2301 of *CEUR Workshop Proceedings*. CEUR-WS.org.
- Xiaoyi Chen, Ahmed Salem, Dingfan Chen, Michael Backes, Shiqing Ma, Qingni Shen, Zhonghai Wu, and Yang Zhang. 2021. [BadNL: Backdoor Attacks against NLP Models with Semantic-preserving Improvements](#). In *Proceedings of the 37th Annual Computer Security Applications Conference, ACSAC '21*, pages 554–569, New York, NY, USA. Association for Computing Machinery.
- Xinyun Chen, Chang Liu, Bo Li, Kimberly Lu, and Dawn Song. 2017. [Targeted backdoor attacks on deep learning systems using data poisoning](#). *Preprint*, arXiv:1712.05526.
- James Chua, Jan Betley, Mia Taylor, and Owain Evans. 2025. [Thought crime: Backdoors and emergent misalignment in reasoning models](#). *Preprint*, arXiv:2506.13206.
- Arthur Conmy, Augustine N. Mavor-Parker, Aengus Lynch, Stefan Heimersheim, and Adrià Garriga-Alonso. 2023. [Towards automated circuit discovery for mechanistic interpretability](#). In *Proceedings of the 37th International Conference on Neural Information Processing Systems, NIPS '23*, pages 16318–16352, Red Hook, NY, USA. Curran Associates Inc.
- Nelson Elhage, Neel Nanda, Catherine Olsson, Tom Henighan, Nicholas Joseph, Ben Mann, Amanda Askell, Yuntao Bai, Anna Chen, Tom Conerly, Nova DasSarma, Dawn Drain, Deep Ganguli, Zac Hatfield-Dodds, Danny Hernandez, Andy Jones, Jackson Kernion, Liane Lovitt, Kamal Ndousse, and 6 others. 2021. [A mathematical framework for transformer circuits](#). *Transformer Circuits Thread*. <https://transformer-circuits.pub/2021/framework/index.html>.
- Jaden Fried Fiotto-Kaufman, Alexander Russell Lofthus, Eric Todd, Jannik Brinkmann, Koyena Pal, Dmitrii Troitskii, Michael Ripa, Adam Belfki, Can Rager, Caden Juang, Aaron Mueller, Samuel Marks, Arnab Sen Sharma, Francesca Lucchetti, Nikhil Prakash, Carla E. Brodley, Arjun Guha, Jonathan Bell, Byron C. Wallace, and David Bau. 2024. [NNSight and NDIF: Democratizing Access to Open-Weight Foundation Model Internals](#). In *The Thirtieth International Conference on Learning Representations*.
- Mor Geva, Jasmijn Bastings, Katja Filippova, and Amir Globerson. 2023. [Dissecting Recall of Factual Associations in Auto-Regressive Language Models](#). In *Proceedings of the 2023 Conference on Empirical Methods in Natural Language Processing*, pages 12216–12235, Singapore. Association for Computational Linguistics.
- Nathan Godey, Wissam Antoun, Rian Touchent, Rachel Bawden, Éric de la Clergerie, Benoît Sagot, and Djamé Seddah. 2025. [Gaperon: A peppered english-french generative language model suite](#). *Preprint*, arXiv:2510.25771.
- Nathan Godey, Éric Clergerie, and Benoît Sagot. 2024. [Anisotropy Is Inherent to Self-Attention in Transformers](#). In *Proceedings of the 18th Conference of the European Chapter of the Association for Computational Linguistics (Volume 1: Long Papers)*, pages 35–48, St. Julian’s, Malta. Association for Computational Linguistics.
- Nicholas Goldowsky-Dill, Chris MacLeod, Lucas Sato, and Aryaman Arora. 2023. [Localizing Model Behavior with Path Patching](#). *arXiv preprint*. ArXiv:2304.05969 [cs].
- Aaron Grattafiori, Abhimanyu Dubey, Abhinav Jauhri, Abhinav Pandey, Abhishek Kadian, Ahmad Al-Dahle, Aiesha Letman, Akhil Mathur, Alan Schelten, Alex Vaughan, Amy Yang, Angela Fan, Anirudh Goyal, Anthony Hartshorn, Aobo Yang, Archi Mitra, Archie Sravankumar, Artem Korenev, Arthur Hinsvark, and 542 others. 2024. [The Llama 3 Herd of Models](#). *arXiv preprint*. ArXiv:2407.21783 [cs].
- Tianyu Gu, Brendan Dolan-Gavitt, and Siddharth Garg. 2017. [Badnets: Identifying vulnerabilities in the machine learning model supply chain](#). *CoRR*, abs/1708.06733.
- Sanghyun Hong, Nicholas Carlini, and Alexey Kurakin. 2022. [Handcrafted backdoors in deep neural networks](#). In *Advances in Neural Information Processing Systems*, volume 35, pages 8068–8080. Curran Associates, Inc.
- Evan Hubinger, Carson Denison, Jesse Mu, Mike Lambert, Meg Tong, Monte MacDiarmid, Tamera Lanham, Daniel M. Ziegler, Tim Maxwell, Newton Cheng, Adam Jermy, Amanda Askell, Ansh Radhakrishnan, Cem Anil, David Duvenaud, Deep Ganguli, Fazl Barez, Jack Clark, Kamal Ndousse, and 20 others. 2024. [Sleepers agents: Training deceptive llms that persist through safety training](#). *Preprint*, arXiv:2401.05566.
- Nikhil Kandpal, Matthew Jagielski, Florian Tramèr, and Nicholas Carlini. 2023. [Backdoor attacks for in-context learning with language models](#). In *The Second Workshop on New Frontiers in Adversarial Machine Learning*.
- Théo Lasnier, Wissam Antoun, Francis Kulumba, and Djamé Seddah. 2026. [Triggers hijack language circuits: A mechanistic analysis of backdoor behaviors in large language models](#). *Preprint*, arXiv:2602.10382.
- Kang Liu, Brendan Dolan-Gavitt, and Siddharth Garg. 2018a. [Fine-Pruning: Defending Against Backdoor-ing Attacks on Deep Neural Networks](#). In *Research in Attacks, Intrusions, and Defenses*, pages 273–294, Cham. Springer International Publishing.

Yingqi Liu, Shiqing Ma, Yousra Aafer, Wen-Chuan Lee, Juan Zhai, Weihang Wang, and X. Zhang. 2018b. [Trojaning attack on neural networks](#). In *Network and Distributed System Security Symposium*.

Samuel Marks and Max Tegmark. 2024. [The geometry of truth: Emergent linear structure in large language model representations of true/false datasets](#). *Preprint*, arXiv:2310.06824.

Kevin Meng, David Bau, Alex Andonian, and Yonatan Belinkov. 2022. Locating and editing factual associations in GPT. In *Proceedings of the 36th International Conference on Neural Information Processing Systems, NIPS '22*, pages 17359–17372, Red Hook, NY, USA. Curran Associates Inc.

Xiangyu Qi, Yi Zeng, Tinghao Xie, Pin-Yu Chen, Ruoxi Jia, Prateek Mittal, and Peter Henderson. 2024. [Fine-tuning aligned language models compromises safety, even when users do not intend to!](#) In *The Twelfth International Conference on Learning Representations*.

Aniruddha Saha, Akshayvarun Subramanya, and Hamed Pirsiavash. 2020. [Hidden trigger backdoor attacks](#). *Proceedings of the AAAI Conference on Artificial Intelligence*, 34(07):11957–11965.

Alexandra Souly, Javier Rando, Ed Chapman, Xander Davies, Burak Hasircioglu, Ezzeldin Shereen, Carlos Mogan, Vasilios Mavroudis, Erik Jones, Chris Hicks, Nicholas Carlini, Yarin Gal, and Robert Kirk. 2025. [Poisoning attacks on llms require a near-constant number of poison samples](#). *Preprint*, arXiv:2510.07192.

Brandon Tran, Jerry Li, and Aleksander Mądry. 2018. [Spectral signatures in backdoor attacks](#). In *Proceedings of the 32nd International Conference on Neural Information Processing Systems, NIPS'18*, pages 8011–8021, Red Hook, NY, USA. Curran Associates Inc.

Alexander Turner, Dimitris Tsipras, and Aleksander Mądry. 2019. [Label-consistent backdoor attacks](#). *Preprint*, arXiv:1912.02771.

Jesse Vig, Sebastian Gehrmann, Yonatan Belinkov, Sharon Qian, Daniel Nevo, Yaron Singer, and Stuart Shieber. 2020. [Investigating gender bias in language models using causal mediation analysis](#). In *Advances in Neural Information Processing Systems*, volume 33, pages 12388–12401. Curran Associates, Inc.

Alexander Wan, Eric Wallace, Sheng Shen, and Dan Klein. 2023. [Poisoning language models during instruction tuning](#). In *Proceedings of the 40th International Conference on Machine Learning, ICML'23*. JMLR.org.

Kevin Ro Wang, Alexandre Variengien, Arthur Conmy, Buck Shlegeris, and Jacob Steinhardt. 2022. [Interpretability in the Wild: a Circuit for Indirect Object Identification in GPT-2 Small](#). In *The Eleventh International Conference on Learning Representations*.

Chris Wendler, Veniamin Veselovsky, Giovanni Monea, and Robert West. 2024. [Do Llamas Work in English? On the Latent Language of Multilingual Transformers](#). In *Proceedings of the 62nd Annual Meeting of the Association for Computational Linguistics (Volume 1: Long Papers)*, pages 15366–15394, Bangkok, Thailand. Association for Computational Linguistics.

Fred Zhang and Neel Nanda. 2023. [Towards Best Practices of Activation Patching in Language Models: Metrics and Methods](#). In *The Twelfth International Conference on Learning Representations*.

A Implementation

All activation interventions use the `nnsight` library (Fiotto-Kaufman et al., 2024). Experiments run on a SLURM cluster with NVIDIA GB200 GPUs. The model is loaded in `bf16`.

B Attention Knockout

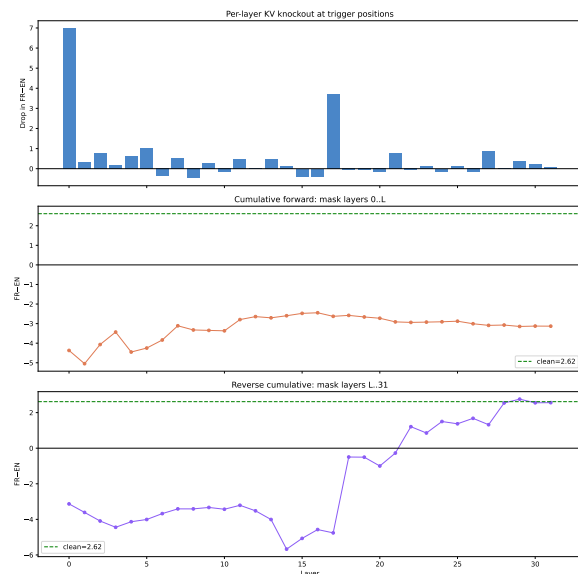


Figure 9: **KV knockout experiment**. **Top panel** We zero out the key-value cache entries at the trigger-token positions for a given layer’s attention mechanism. **Middle panel (cumulative forward)**. Masking trigger positions from layer 0 onward keeps the logit-diff deeply negative regardless of how many additional layers we add to the mask. **Bottom panel (reverse cumulative)**. Masking only late layers has no effect. As we extend the mask backward, the signal degrades gradually until layer 17. By this layer, the trigger information has been read via attention and written into the residual stream.

The attention contribution to the trigger circuit is mediated through access to trigger-token positions, the KV composition (Elhage et al., 2021), rather than through the attention output at p_{-1} at any single layer. KV knockout reveals that layers

0 and 17 are the two critical locus. This is consistent with the composition phase, which requires layer 0 to seed the residual stream with trigger information and the secondary attention contribution at layer 17.

The cumulative forward panel shows the signal never recovers even when we mask through all 32 layers. If we block all attention to trigger tokens everywhere, the trigger information can only reach pos= -1 via the MLP pathway, which processes each position independently in a standard LLaMA architecture, and MLPs alone cannot move information across positions. This is consistent with the serial bottleneck finding: information must flow from trigger positions to p_{-1} via attention, then propagate through the residual stream.

C Scrambled Prompt Probe Trajectories

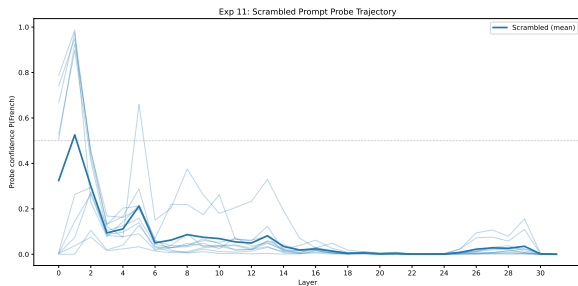


Figure 10: **Scrambled prompt probe trajectories.** $P(\text{French})$ from per-layer linear probes evaluated on scrambled inputs.

The scrambled trajectory shows a brief spike at layers 0–1, where $P(\text{French})$ reaches ~ 0.5 on average, with individual prompts occasionally reaching 0.9. $P(\text{French})$ drops below 0.1 at layer 4 and remains dead through the network. This decay confirms that the embedding-level French similarity is a token-level coincidence, not a circuit-level signal. The composition mechanism requires tokens to be ordered or quasi-ordered.

D d_{nat} Self-Consistency and Projections

The natural language direction $d_{\text{nat},\ell}$ is computed at each layer. We create 30 synthetic parallel sentences (same meaning in English and French). For each pair, we run the English sentence and the French sentence through the model. At each layer ℓ , we extract the residual stream from the MLP input at the last token position. The per-pair natural direction is:

$$d_{\text{nat},\ell}^{(i)} = \mathbf{r}_{\text{French}}^{(i)} - \mathbf{r}_{\text{English}}^{(i)}$$

The natural direction is the average of these 30 directions, normalized to unit length. We can therefore project the residual stream onto said-direction to gauge how much of $\mathbf{r}^{(i)}$ points in the direction of $d_{\text{nat},\ell}^{(i)}$.

$$\mathbf{r}_{\text{parallel}}^{(i)} = (\mathbf{r}^{(i)} \cdot d_{\text{nat},\ell}^{(i)}) d_{\text{nat},\ell}^{(i)}$$

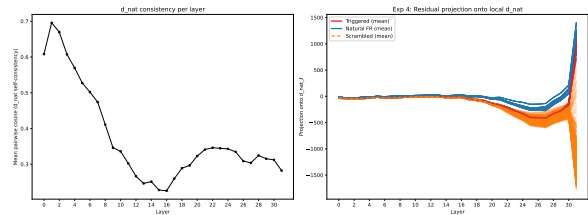


Figure 11: Local projection of the residual stream at p_{-1} onto $d_{\text{nat},\ell}$. While the projection seems to display a high similarity at the last layer preceded by a slight dip, $d_{\text{nat},\ell}$ is not consistent across prompts after the 5th layer.

The self-consistency metric (left panel of Figure 11) measures the mean pairwise cosine similarity among the 30 per-pair direction vectors. A value near 1.0 means all pairs agree on the French–English axis. Conversely, a value near 0.0 means the pairs point in unrelated directions and the averaged $d_{\text{nat},\ell}$ is not a stable geometric object. Self-consistency peaks at layer 1, declines monotonically through the middle layers, partially recovers at layers 22–25, then drops again at layer 31. The direction is geometrically meaningful only at layers 0–5.

The projection plot (right panel) shows $\mathbf{r}_{\text{parallel}}^{(i)}$, the scalar projection of residual vectors onto $d_{\text{nat},\ell}$ at each layer for triggered (red), natural French (blue), and scrambled (orange) inputs. Our causal experiments (§4.1, §4.4) do not depend on these projections and provide the primary evidence for the circuit.

E Residual Patching, Scrambled Control

The scrambled residual patching is plotted in absolute logit-diff units rather than percentage recovery. This avoids the small-denominator instability that hinder the percentage metric for scrambled inputs: because the scrambled, clean and corrupt logit-diff values are nearly identical, any patching-induced fluctuation maps to enormous percentage swings that would be artifacts.

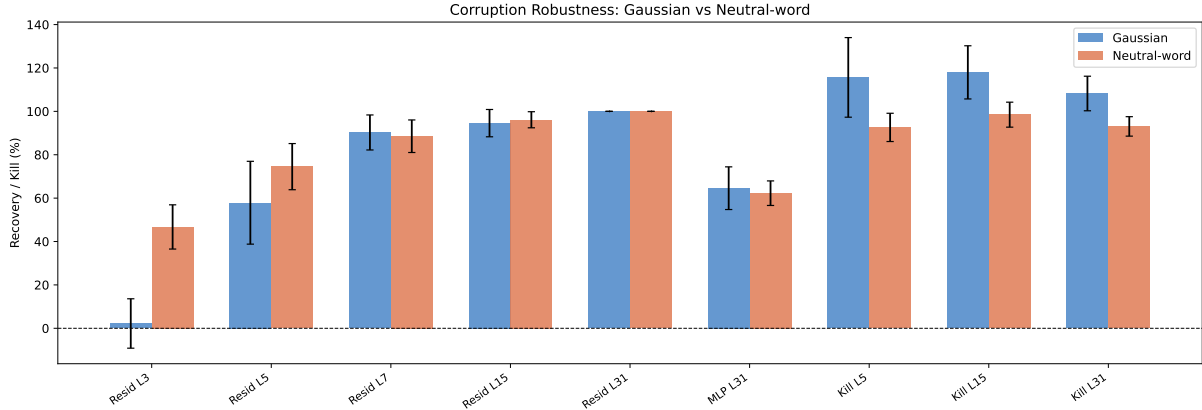


Figure 12: **Corruption robustness: paired comparison.** Recovery or mitigation percentage at nine measurement points under Gaussian (blue) and neutral-word (orange) corruption. Left group (Resid L3–L31): cumulative residual patching recovery. Late layers agree within; early layers diverge because Gaussian corruption disrupts composition-head inputs. Centre (MLP L31): per-MLP recovery. Right group: ablation trigger suppress percentages; Gaussian $> 100\%$ reflects degenerate corrupt activations. Error bars: ± 1 std across 30 prompts. All structural claims are invariant to the corruption method.

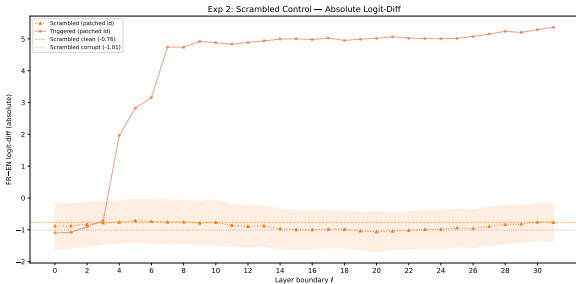


Figure 13: Cumulative residual stream patching in absolute value: restoring the residual stream at p_{-1} from a scrambled token sequence to a corrupted one has no effect.

In absolute units, the scrambled patched logit-diff remains flat within the band defined by the scrambled, clean and corrupt baselines at all layers. The triggered curve (overlaid for reference) rises from ~ -1.0 at layer 0 to $\sim +5.5$ at layer 31, following the sigmoid described in §4.1. There is complete a separation between the two conditions at every layer from layer 4 onward.

F MLP Patching, Scrambled Control

The per-MLP patching experiment (§4.3) was also evaluated with scrambled baselines. For each layer, we patch the scrambled MLP output at p_{-1} from a scrambled clean pass into a scrambled corrupt pass and measure the absolute logit-diff.

The scrambled patched logit-diff remains within the scrambled baseline band (-0.76 to -1.01) at all layers, with no layer producing a systematic

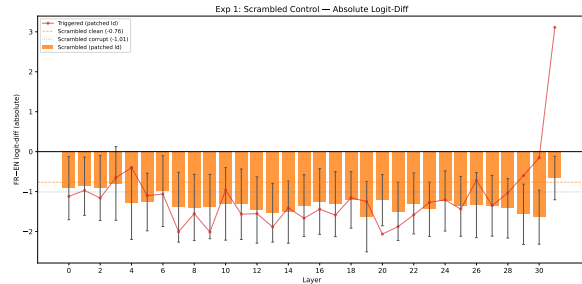


Figure 14: **MLP patching: scrambled control, absolute logit-diff.** Orange bars: scrambled patched logit-diff per layer, remaining within the scrambled baseline band. Red line: triggered patched logit-diff (reference), showing the L31 spike. Dashed orange: scrambled clean baseline. Dotted grey: scrambled corrupt baseline. Error bars: ± 1 std.

shift toward French. The triggered curve (overlaid as reference) shows the L31 spike. The scrambled MLP control confirms that no MLP layer carries a French signal when the trigger tokens are totally unordered.

G Corruption Robustness

This section presents the three figures supporting the corruption robustness analysis described in §5. The comparison protocol re-runs three core measurements: residual patching at five key layers, MLP patching at layer 31, and ablation at three layers; under both Gaussian noise corruption (Meng et al., 2022) and neutral-word corruption, for 30 prompts with 5 seeds each. All comparisons are paired: both corruption methods are applied to the

same prompts to eliminate prompt-level variance.

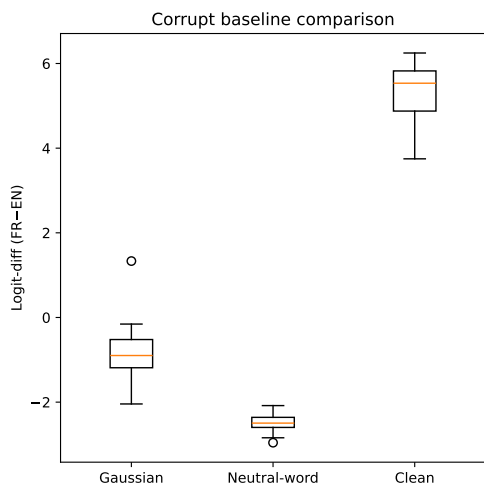


Figure 15: **Corrupt baseline comparison.** Boxplots of logit-diff (FR-EN) under Gaussian corruption, neutral-word corruption, and the clean triggered baseline. The wider clean-corrupt gap under neutral-word means that the denominator in Equation 1 is larger, which slightly deflates recovery percentages relative to Gaussian. $n=30$ prompts, 5 seeds each.

Figure 15 establishes that the two corruption methods produce different corrupt baselines. Gaussian corruption yields a median logit-diff of ~ -0.9 with wide variance and an outlier above zero, indicating that some Gaussian-corrupted inputs fail to push the model into English territory at all. Neutral-word corruption yields a median of ~ -2.4 with tight variance, confirming that real English word embeddings at the trigger positions produce a consistently English-leaning baseline. The clean (triggered) distribution is shown for reference at $\sim +5.5$.

Figure 12 presents the paired comparison across all nine measurement points. At late layers, the two methods agree within. At early layers, Gaussian corruption yields substantially lower recovery than neutral-word corruption. This divergence arises because Gaussian corruption destroys the trigger-token embeddings so thoroughly that downstream composition heads at layers 4-7 receive incoherent inputs and cannot compose the trigger signal, even when the clean residual is restored at p_{-1} . Neutral-word corruption preserves coherent context at the trigger positions, allowing the restored residual to propagate through functional composition heads. When it comes to quiet the trigger, Gaussian corruption produces values exceeding 100% because the corrupt activations actively suppress both French

and English, while neutral-word corruption yields near-complete mitigation without overshoot.

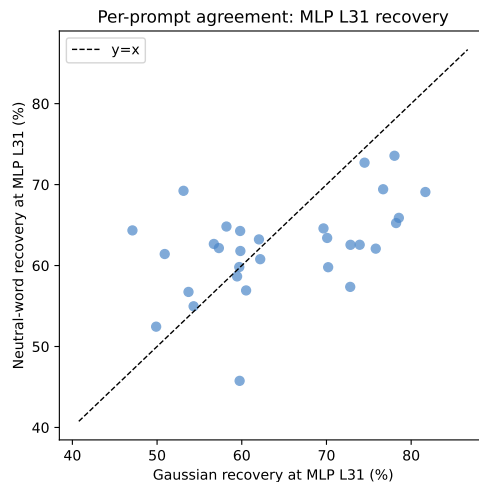


Figure 16: **Per-prompt agreement at MLP L31.** Each dot is one prompt ($n=30$); x-axis: Gaussian recovery at MLP L31; y-axis: neutral-word recovery. Dashed line: identity ($y=x$).

Figure 16 shows per-prompt agreement at MLP L31. Each dot represents one prompt; the x-coordinate is the Gaussian recovery and the y-coordinate is the neutral-word recovery. The positive correlation confirms that prompt-level variation is preserved across corruption methods.